



# Conformation-sensitive targeting of lipid nanoparticles for RNA therapeutics

Niels Dammes<sup>1,2,3,4</sup>, Meir Goldsmith<sup>1,2,3,4</sup>, Srinivas Ramishetti<sup>1,2,3,4</sup>, Jason L. J. Dearling<sup>5,6</sup>, Nuphar Veiga<sup>1,2,3,4</sup>, Alan B. Packard<sup>5,6</sup> and Dan Peer<sup>1,2,3,4</sup> ✉

**The successful in vivo implementation of gene expression modulation strategies relies on effective, non-immunogenic delivery vehicles. Lipid nanoparticles are one of the most advanced non-viral clinically approved nucleic-acid delivery systems. Yet lipid nanoparticles accumulate naturally in liver cells upon intravenous administration, and hence, there is an urgent need to enhance uptake by other cell types. Here we use a conformation-sensitive targeting strategy to achieve in vivo gene silencing in a selective subset of leukocytes and show potential therapeutic applications in a murine model of colitis. In particular, by targeting the high-affinity conformation of  $\alpha_4\beta_7$  integrin, which is a hallmark of inflammatory gut-homing leukocytes, we silenced interferon- $\gamma$  in the gut, resulting in an improved therapeutic outcome in experimental colitis. The lipid nanoparticles did not induce adverse immune activation or liver toxicity. These results suggest that our lipid nanoparticle targeting strategy might be applied for selective delivery of payloads to other conformation-sensitive targets.**

Inflammatory bowel disease (IBD) is a growing problem with rising incidence since the 19th century. Despite several decades of research in both animals and humans, current treatments remain disappointing and do not provide a cure<sup>1</sup>. Although novel biologics such as antibodies against TNF- $\alpha$  have revolutionized IBD treatment, not all patients respond, and initial responders can lose response over time due to the development of anti-drug antibody (ADA<sup>2,3</sup>) responses.

To establish a curative solution to IBD, blocking cytokines or receptors with antibodies is most likely insufficient and provides only temporary relief from the symptoms. A curative solution could be achieved by actively modulating gene expression in the aberrantly activated leukocyte population. Altering the expression of specific genes in inflammatory leukocytes and thereby changing their behaviour might restore the balance in the intestinal immune response over the longer term. The feasibility of this is supported by several studies that demonstrated modulation of gene expression by, for instance, silencing TNF- $\alpha$  (ref. <sup>4</sup>) or overexpressing IL-10 (ref. <sup>5</sup>) in a specific subset of cells in experimental colitis. These studies relied on the use of lipid nanoparticles (LNPs) to deliver therapeutic nucleic acids in vivo (Fig. 1a). LNPs have evolved over the years to become one of the most suitable non-viral methods of delivering nucleic acids in vivo due to their high encapsulation efficiency, low batch-to-batch variation and fusogenic properties<sup>6,7</sup>. Since the recent approval of the first-ever RNA interference-based drug, Onpatro (patisiran), by the FDA<sup>8</sup>, the use of LNPs has gained even more momentum. Like most injected particulates, LNPs tend to accumulate in the liver and are thereby limited in their use in other cell types. Recent attempts to generate targeted LNPs that, in addition to accumulating in the liver, are directed to other cells as well<sup>4,5,9</sup> generated promising results and opened the door to a new era of targeted delivery of therapeutic nucleic acids.

Herein, we report the delivery of siRNAs specifically to activation-sensitive receptors expressed on gut-homing leukocytes in a mouse model of colitis. Our targeting strategy is different from traditional strategies as we employ a targeting moiety that only recognizes a specific protein conformation, namely the high-affinity (HA) conformation of integrin  $\alpha_4\beta_7$ . Gut-homing leukocytes utilize this pivotal intestinal homing receptor to adhere to the intestinal endothelium. Previously, we exploited this leukocyte integrin and generated lipid nanoparticles that were targeted to the  $\beta_7$  integrin subunit<sup>10</sup>. Although  $\alpha_4\beta_7$  integrin is considered a key protein in homing of leukocytes to the gut during intestinal inflammations, in healthy individuals, ~70% of the total intestinal T-cell population and ~35% of circulating CD4<sup>+</sup> T cells express  $\alpha_4\beta_7$  integrin<sup>11</sup>, indicating that merely targeting  $\alpha_4\beta_7$  integrin or one of its subunits lacks specificity.

Integrin functionality depends on the conformational state<sup>12</sup>. Integrins change conformation when stimulated and dramatically increase the affinity for their ligands. Integrin  $\alpha_4\beta_7$  has the potential to bind both vascular cell adhesion molecule-1 (VCAM-1) for homing to peripheral tissues and MAdCAM-1 for homing to intestinal tissues, but not simultaneously. Whether integrin  $\alpha_4\beta_7$  has affinity for VCAM-1 or MAdCAM-1 depends on the specific stimulus, subsequent signalling and type of conformational change<sup>13</sup>. As only leukocytes that actively home to the intestinal tissues possess  $\alpha_4\beta_7$  integrin in the HA conformation, we wanted to generate LNPs that can target integrin  $\alpha_4\beta_7^+$ -expressing cells in a conformation-dependent manner (Fig. 1e). This is contrary to commercially available conformation-insensitive monoclonal antibodies (mAbs) such as natalizumab (anti- $\alpha_4$  integrin) and vedolizumab (anti- $\alpha_4\beta_7$  integrin). The possible danger associated with insufficient specificity when blocking leukocyte homing is exemplified by natalizumab, which was temporally withdrawn from the market for

<sup>1</sup>Laboratory of Precision Nanomedicine, Shmunis School of Biomedicine and Cancer Research, George S. Wise Faculty of Life Sciences, Tel Aviv University, Tel Aviv, Israel. <sup>2</sup>Department of Materials Sciences and Engineering, Iby and Aladar Fleischman Faculty of Engineering, Tel Aviv University, Tel Aviv, Israel. <sup>3</sup>Center for Nanoscience and Nanotechnology, Tel Aviv University, Tel Aviv, Israel. <sup>4</sup>Cancer Biology Research Center, Tel Aviv University, Tel Aviv, Israel. <sup>5</sup>Division of Nuclear Medicine and Molecular Imaging, Department of Radiology, Boston Children's Hospital, Boston, MA, USA. <sup>6</sup>Harvard Medical School, Boston, MA, USA. ✉e-mail: [peer@tauex.tau.ac.il](mailto:peer@tauex.tau.ac.il)

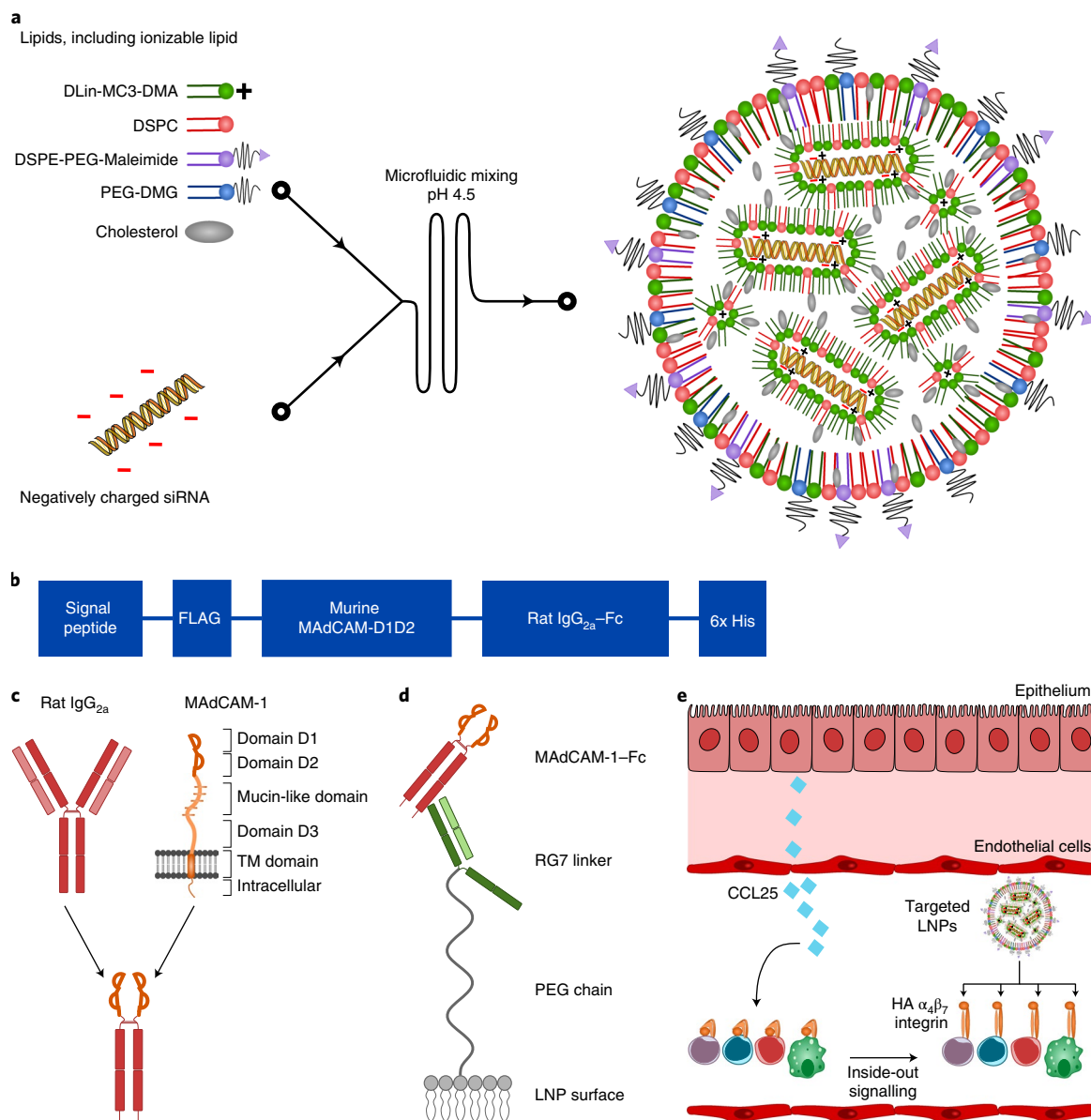


**Fig. 1 | Generation of LNPs to target the high-affinity conformation of integrin  $\alpha_4\beta_7$ .** **a**, Illustration of the generation of LNPs using microfluidics. The ionizable lipid facilitates short interfering RNA (siRNA) encapsulation through its positive charge at low pH. **b**, Overview of the different domains of the mucosal vascular addressin cell adhesion molecule-1 (MAdCAM-1)-Fc fusion protein. **c**, Overview of the fusion strategy. The different domains of the wild-type MAdCAM-1 are shown. Only the integrin binding domains D1 and D2 are used. D1D2 is fused to the hinge of rat IgG<sub>2a</sub> with a flexible linker. **d**, Schematic drawing depicting the conjugation strategy of the MAdCAM-1-Fc to the LNPs. The RG7 linker (mAb against rat IgG<sub>2a</sub>) is chemically conjugated with the LNPs to the maleimide group in the lipid DSPE-PEG-maleimide. RG7 readily binds the MAdCAM-1-Fc by antibody affinity. **e**, LNP targeting to HA  $\alpha_4\beta_7$  integrin. CCL25 induces the integrin conformational change.

treatment of IBD due to increased risk of opportunistic infections leading to multifocal leukoencephalopathy<sup>14</sup>.

In this study, we generated a recombinant fusion protein that contains two domains of the intestinal endothelium ligand MAdCAM-1. MAdCAM-1 naturally has an increased affinity to integrin  $\alpha_4\beta_7$  in its HA conformation and is therefore an excellent start for the design of the LNP targeting moiety. MAdCAM-1 is a multi-domain protein that is naturally involved in both initial tethering and firm adhesion of leukocytes to the intestinal endothelium.

To maximize specificity, we only utilized the integrin binding domains D1 and D2 (Fig. 1b,c). To protect the integrin binding domain while conjugating the protein to the LNPs, we made use of a monoclonal secondary antibody against rat IgG<sub>2a</sub>, here referred to as RG7,

which serves as a linker between the LNPs and the MAdCAM-D1D2 protein. The RG7 linker was chemically conjugated to the LNPs using maleimide/thiol chemistry and the MAdCAM-D1D2 protein was recombinantly fused to the Fc region of rat IgG<sub>2a</sub>. This way, the RG7 antibody will bind the MAdCAM-1 protein by affinity to the rat IgG<sub>2a</sub> domain and leave the domains D1 and D2 free for binding to  $\alpha_4\beta_7$  integrin (Fig. 1d). This conjugation strategy was compared with two other options: direct conjugation to the DSPE-PEG-maleimide lipid using reduced cysteine residues in the D1D2 protein or by using a previously published conjugation strategy that involves anchored secondary scFv enabling targeting (ASSET; scFv stands for single-chain variable fragment), a lipidated scFv against rat IgG<sub>2a</sub> that readily incorporates in the LNPs<sup>4</sup>. When ASSET is incorporated into the

LNPs, it can bind the D1D2–Fc by affinity. For our specific approach, the RG7-mediated conjugation was far superior to the other two methods (Supplementary Fig. 1). We ensured that this linkage was sufficiently stable in freshly isolated mouse blood plasma for at least 1 hour at 37 °C (Supplementary Fig. 2).

**Design and production of MAdCAM-1–Fc protein.** The domains D1 and D2 of murine MAdCAM-1 were fused to the N terminus of the Fc domain of rat IgG<sub>2a</sub> (including hinge, excluding C<sub>H1</sub>). A signal peptide for secretion and a FLAG tag were added to the N terminus of the construct and a 6x His tag was added at the C terminus for purification purposes. Purity and size (~50 kDa) were confirmed by SDS–polyacrylamide gel electrophoresis (SDS–PAGE) (Fig. 2a).

We also generated a mutated version of the MAdCAM-1–D1D2–Fc that serves as a negative control. This has the D42A mutation that has been reported to severely affect the ability of MAdCAM-1 to bind  $\alpha_4\beta_7$  integrin<sup>15</sup>. This mutation affects the amino-acid sequence LDTs, which has been shown to be the critical motif that is actively engaged in integrin binding<sup>16</sup>. In the rest of this manuscript, we use D1D2 to refer to the non-mutated version and mD1D2 to refer to the mutated version.

After purifying D1D2 and mD1D2, we tested the functionality *in vitro* by assessing the binding to TK-1 cells using flow cytometry. TK-1 cells have been shown to express high levels of  $\alpha_4\beta_7$  integrin<sup>10,17</sup> and are therefore an excellent *in vitro* model for testing the functionality of the recombinant MAdCAM-1 construct. Cells were either treated with Mn<sup>2+</sup> to create the HA- $\alpha_4\beta_7$  or with Ca<sup>2+</sup> as an LA- $\alpha_4\beta_7$  control. As expected, in the absence of Mn<sup>2+</sup>, no difference in cell binding between D1D2 and mD1D2 was observed; however, a significant difference ( $P < 0.0001$ ,  $n = 4$ ) in binding was visible upon Mn<sup>2+</sup> treatment (Fig. 2b).

After validating that the D1D2 protein binds exclusively to the HA conformation of integrin  $\alpha_4\beta_7$ , we used molecular imaging to analyse the biodistribution. We have previously reported that targeting  $\beta_7$  integrin and  $\alpha_4\beta_7$  integrin via mAbs facilitates specific imaging of inflammatory leukocytes in dextran sulfate sodium (DSS) colitis (although unspecific accumulation in the liver cannot be excluded)<sup>18,19</sup>. Here we wanted to test this with the newly developed D1D2 targeting protein, so we performed a proof-of-concept study on the imaging of inflammatory leukocytes in experimental colitis. We conjugated the D1D2 protein directly to a chelator, NOTA, to enable labelling with the radioisotope <sup>64</sup>Cu. This did not affect the protein functionality, as validated by binding to TK-1 cells (Fig. 3a).

D1D2–NOTA–<sup>64</sup>Cu or mD1D2–NOTA–<sup>64</sup>Cu was injected into both healthy mice and mice with colitis, and 24 h post injection, the mice were imaged by microPET/CT. Injection of the radio-labelled D1D2 protein did not affect the colitis severity (Fig. 3b). Figure 3c displays a representative image of the biodistribution. The D1D2–NOTA–<sup>64</sup>Cu shows an increased uptake in the gut of colitic mice. This uptake was significantly correlated to colitis severity (Supplementary Fig. 6) with  $n = 5$  mice per group ( $P = 0.014$ ). Colon density was used to score colitis severity. This experiment lacked extensive colitis scoring such as histology, but we believe that it still gives a good indication of preferential uptake of D1D2 in the inflamed colons.

**Generation of targeted LNPs.** Having confirmed the binding of D1D2 to gut-tropic leukocytes, we generated targeted LNPs. To generate uniformly sized LNPs that have a high siRNA encapsulation efficiency and minimal batch-to-batch variation, we used the NanoAssemblr microfluidic mixing device<sup>20</sup>. The ionizable lipid DLin–MC3–DMA aids in siRNA encapsulation as has previously been reported<sup>21</sup>, and we used an LNP formulation that we and others have previously reported<sup>4,5,22</sup>.

LNPs had a mean diameter of ~40 nm, zeta potentials of approximately –10 mV (Fig. 2e) and encapsulation efficiencies close to 90%

(Fig. 2d). The size and uniformity of the particles was confirmed using transmission electron microscopy (Fig. 2c).

The LNPs were conjugated to RG7 using maleimide–thiol chemistry. The targeting protein is bound to the LNP surface through affinity by the RG7 linker.

The biodistribution of the targeted LNPs was analysed by microPET/CT. We covalently added a TCO group to the DSPE–PEG lipid to enable TCO–tetrazine chemistry to add the chelator (NOTA). However, we did not see increased uptake in target tissue compared with controls (Supplementary Fig. 5). Large macromolecules such as LNPs accumulate in the liver, and it is hard to clearly distinguish enhanced uptake in other tissues. Furthermore, tissue-specific targeting is often dependent on passive targeting. Only once the tissue of interest is reached can LNPs take advantage of the increased affinity of targeting moieties by binding and internalizing to specific cells<sup>23</sup>. It is therefore hard to distinguish tissue distribution between the D1D2-targeted and the mD1D2-targeted LNPs. The targeting is mainly related to enhanced cell-specific uptake rather than the alteration of tissue accumulation by the LNPs.

After preparation, conjugation and purification of the LNPs, the functionality of the D1D2-targeted LNPs was tested. Binding of LNPs to cells (Mn<sup>2+</sup>- or Ca<sup>2+</sup>-treated) was tested by flow cytometry using encapsulated Cy5–siRNA that can fluorescently label bound cells. As shown in Fig. 2f, LNP binding increased dramatically when targeted by D1D2 as compared to mD1D2. Furthermore, confocal microscopy indicated internalization of the Cy5-labelled, D1D2-targeted LNPs (Fig. 2g). D1D2 LNP binding was compared to both mD1D2 and anti- $\alpha_4\beta_7$  integrin (mAb clone DATK32) in primary leukocytes. Specific binding of D1D2 LNPs to Mn<sup>2+</sup>-activated primary cells was evident, while DATK32 was conformation insensitive (Supplementary Fig. 3). D1D2-targeted LNPs bound most robustly to CD4<sup>+</sup> T cells from the mesenteric lymph node (mLN) in a conformation-dependent manner.

Chemokine (C–C motif) ligand 25 (CCL25) specifically increases  $\alpha_4\beta_7$  integrin's affinity for MAdCAM-1 by binding to the CCR9 receptor. As expected, CCL25 treatment of cells enhances D1D2 LNP binding compared to CXCL10-treated control cells (CXCL10 increases  $\alpha_4\beta_7$  integrin's affinity for VCAM-1) (Supplementary Fig. 4).

**D1D2 LNPs silence CD45 in conformation-sensitive manner.** Before testing therapeutic gene silencing, feasibility was tested with the pan-leukocyte marker CD45. DSS colitis, a common model, did not result in substantial gene silencing, probably because DSS colitis is strongly macrophage driven and T and B cell independent<sup>24,25</sup>. Therefore, we explored another animal model: piroxicam-accelerated colitis (PAC) in IL-10KO mice<sup>26,27</sup>. Although macrophages play an important role in the PAC model as well<sup>28</sup>, we thought it would be of interest to investigate the effects of targeting a specific subpopulation of CD4<sup>+</sup> T cells in the PAC model. Furthermore, IL-10KO mice with active colitis have strongly increased levels of MAdCAM-1 in the gut<sup>29</sup>, pointing to the importance of MAdCAM-1 in IL-10 deficient mice.

Five days post intravenous injection with siCD45 LNPs, cells from the mLN were collected. Cells from the spleen were also collected as a control, peripheral-lymphoid organ. Cells were analysed for their CD45 expression using flow cytometry (gating strategy shown in Supplementary Fig. 9). Silencing levels in the spleen were negligible, while CD4<sup>+</sup> T cells from mLN were effectively silenced by D1D2-targeted LNPs (Fig. 4a,b). As a negative control, healthy mice were also injected with D1D2-targeted LNPs, yielding no significant results in any cell type from any organ (Fig. 4b).

LNPs did not affect the colitis severity, as was concluded from colon histology in mice from the different groups (Supplementary Fig. 7). No elevation of the liver enzymes aspartate aminotransferase (AST), alanine transaminase (ALT) or alkaline phosphatase (ALP) was detected (Fig. 5c). In addition, liver histology did not

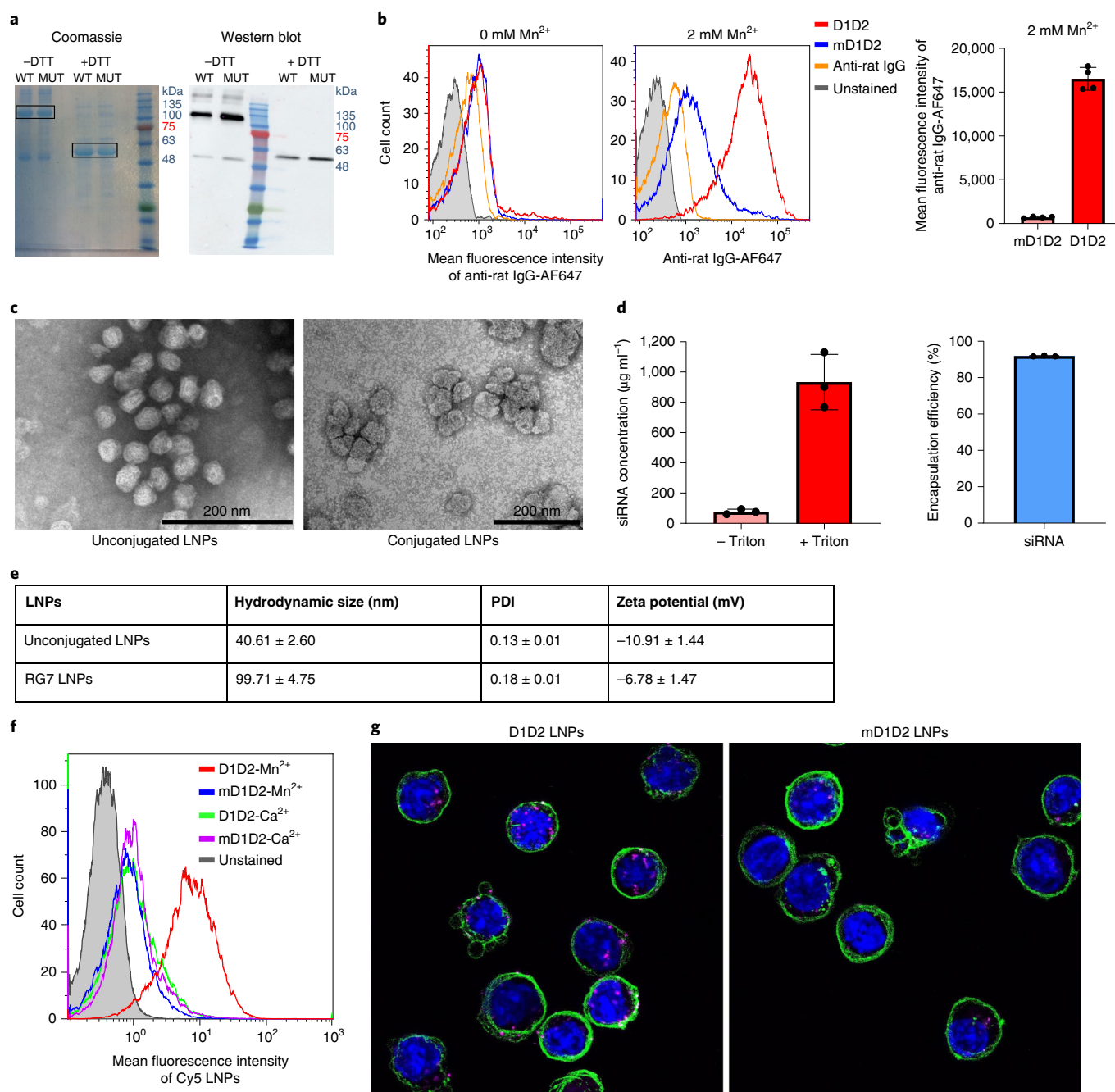


**Fig. 2 | Characterization of D1D2, LNPs and D1D2-targeted LNPs.** **a**, SDS-PAGE of both the D1D2 (WT) and mD1D2 (MUT) proteins. Dimerization through disulfide bonds is evident when comparing to the lanes without reducing agent. Experiment was repeated three times independently. DTT, dithiothreitol. **b**, In vitro binding of the purified D1D2 protein to TK-1 cells measured by flow cytometry. mD1D2 does not bind the cells, while the D1D2 binds only cells with HA integrin  $\alpha_4\beta_7$  (after addition of  $Mn^{2+}$ ). Mean fluorescence intensity of anti-rat IgG-AF647 is in arbitrary units. A significant difference between D1D2 and mD1D2 in  $Mn^{2+}$ -activated cells was observed ( $P < 0.0001$ ;  $n = 4$  biologically independent samples; two-sided Student's  $t$ -test; data are presented as mean  $\pm$  s.d.). **c**, Representative transmission electron microscopy images of unjugated LNPs and LNPs conjugated to RG7. Experiment was repeated three times independently. **d**, siRNA entrapment efficiency assayed by Ribogreen. Bars show mean of  $n = 3$  biologically independent samples; black points show individual samples. Error bars represent  $\pm$  s.d. **e**, Hydrodynamic size, polydispersity index (PDI) and zeta potential of the produced LNPs. Data are presented as mean  $\pm$  s.d. **f**, In vitro binding of Cy5-labelled, D1D2-targeted LNPs to TK-1 cells. **g**, Representative confocal images showing internalization of Cy5-labelled LNPs (magenta) into TK-1 cells. Images were generated by combining 11 frames from z-stack imaging ( $0.3 \mu\text{m}$  per frame).

reveal any excessive bleeding or liver damage (Fig. 5d); thus, we concluded that injection of the LNPs does not cause any observable liver toxicity. Furthermore, the LNPs did not induce unwanted immune responses as measured by complete blood count (Fig. 5b)

and splenic TNF- $\alpha$  and IL-6 expression levels (Fig. 5a). There was no significant difference in counts of the platelets, neutrophils and lymphocytes between the groups, and counts of eosinophils and monocytes in the blood were nearly undetectable.

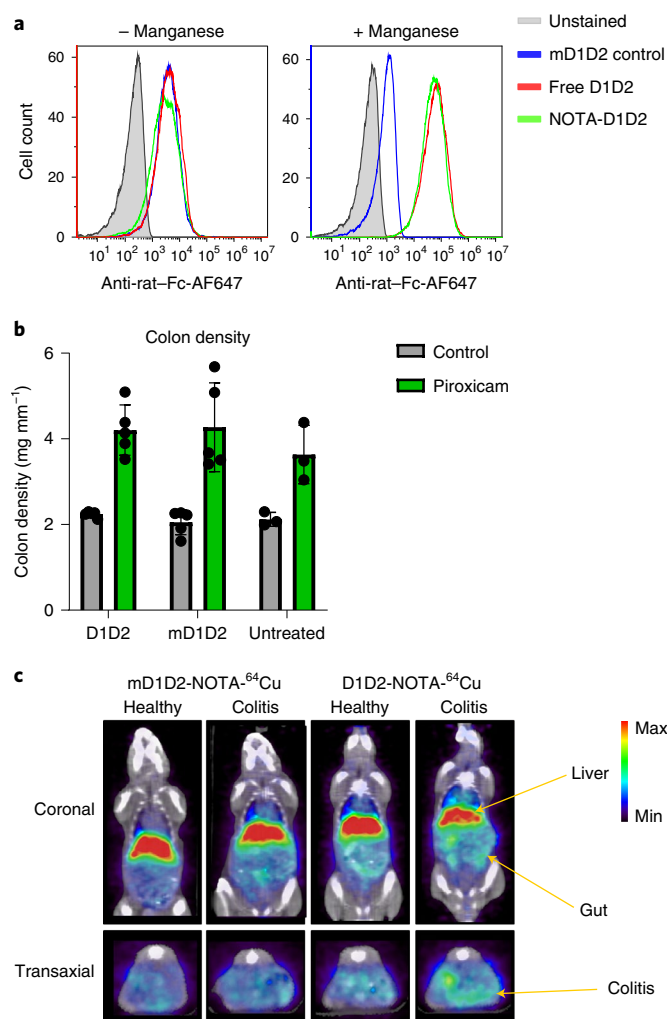


**Fig. 3 | Molecular imaging of inflammatory leukocytes in experimental colitis using positron emission tomography-computed tomography (PET/CT) and D1D2-NOTA-<sup>64</sup>Cu.** **a**, NOTA conjugation with D1D2 did not affect the protein functionality as was demonstrated with binding to TK-1 cells. **b**, Treatment with NOTA-conjugated D1D2 or mD1D2 did not significantly affect colitis severity as determined by colon density (mg tissue per mm penetration) and analysed by one-way analysis of variance (ANOVA). There was a significant difference ( $P=0.0008$ ,  $n=10$  mice) in colon density between piroxicam-treated animals and controls, confirming active colitis. Data are presented as mean values  $\pm$  s.d. **c**, Representative image of PET/CT imaging using D1D2-NOTA-<sup>64</sup>Cu. Gut uptake was compared to mD1D2-NOTA-<sup>64</sup>Cu as control. Colour scale indicates disintegrations per minute.

**Efficacy of siIFN- $\gamma$ -D1D2 LNPs in mice with active colitis.** Based on the CD45 silencing results, a therapeutic target gene related to CD4<sup>+</sup> T-cell biology was explored for therapeutic efficacy studies. Because IFN- $\gamma$  is secreted by inflammatory Th1 cells, and as IFN- $\gamma$  is causatively involved in experimental colitis<sup>30</sup>, this gene was chosen as a therapeutic target gene. To test the therapeutic efficacy, D1D2 LNPs or mD1D2 LNPs loaded with siIFN- $\gamma$  were injected into mice with colitis 4, 6, 8 and 10 days after initiation of colitis (Fig. 6a). A control mouse group injected with D1D2 LNPs loaded with an siNC was used to correct for possible therapeutic effects unrelated to IFN- $\gamma$ . Mice without piroxicam were used as a healthy control, and a validated mAb against TNF- $\alpha$  was used as a positive therapeutic control (administered at days 4, 6, 8 and 10). The antibody against TNF- $\alpha$  was used as a positive control for amelioration

of colitis. Blocking of TNF- $\alpha$  with mAbs has been well validated, and anti-TNF- $\alpha$  mAbs are currently used in the clinic (for example, infliximab<sup>31</sup>). At day 11, mice were killed, and colitis was assessed in all groups (Fig. 6).

Starting from day 8, there was a significant difference in weight change in the D1D2-siIFN- $\gamma$  group as compared to the negative control groups (Fig. 6b). Colonic levels of IFN- $\gamma$  decreased dramatically ( $\sim 2.5$ -fold) in D1D2-targeted IFN- $\gamma$  LNPs as compared to the mD1D2 control (Fig. 6f). Colonic IFN- $\gamma$  levels also decreased in mice treated with the anti-TNF- $\alpha$  antibody, likely due to an overall decrease in intestinal inflammation. Because IFN- $\gamma$  affects TNF- $\alpha$  expression<sup>32</sup> and because these two cytokines have synergistic effects on NF- $\kappa$ B signalling<sup>33</sup>, we would expect an associated reduction of other pro-inflammatory cytokines by silencing IFN- $\gamma$ . Mice treated with D1D2-siIFN- $\gamma$  LNPs and mice treated with anti-TNF- $\alpha$  mAb showed a strong decrease in colonic TNF- $\alpha$  levels (Fig. 6e). The colonic TNF- $\alpha$  levels in mice treated with the mAb against TNF- $\alpha$  (positive control) were even lower than those in the D1D2 LNPs group ( $P<0.05$ ). Furthermore, blood IL-6 and IL-1 $\beta$  levels decreased dramatically and equally in mice treated with both D1D2-targeted LNPs and anti-TNF- $\alpha$  mAb (Fig. 6g,h). Colon length (colon shortening is an important marker of colonic inflammation) was significantly increased ( $P<0.0001$ ) in the D1D2-targeted group as compared to the mD1D2 control (Fig. 6c). A significantly lower colon histological score ( $P<0.0001$ ) further supported the improved therapeutic outcome in mice treated with D1D2-targeted IFN- $\gamma$ -LNPs (Fig. 6d). These results were also in accordance with visual examination of photomicrographs of sections of the colon (Supplementary Fig. 8). Taken together, these data demonstrate a strong therapeutic response in mice treated with D1D2-targeted LNPs loaded with siIFN- $\gamma$ , while the mutated control (mD1D2) did not lead to a significantly improved therapeutic outcome. This approach opens new potential avenues for conformation-sensitive targeting as a novel therapeutic modality with reduced adverse effects and increased efficacy.

## Conclusions

While novel biologics such as mAbs have entered the IBD arena, they lack conformational specificity. Given the chronic nature of IBD and the lifelong dependence on such medications, non-specific treatments could potentially lead to iatrogenic global immune suppression, sensitizing the patient to opportunistic infections. To overcome this, we report here on a strategy to specifically target gut-homing leukocytes in experimental colitis. We fused the integrin binding domains D1 and D2 of the natural ligand of  $\alpha_4\beta_7$  integrin, MADCAM-1, to an IgG-Fc and devised a strategy to efficiently conjugate this fusion protein to the surface of lipid nanoparticles.

We silenced genes in an inflammation-dependent manner in lymphocytes (mainly T cells), cells that are intrinsically hard to transfect. Using siIFN- $\gamma$ , we translated this gene knockdown into an improved therapeutic outcome in IL-10KO mice with active colitis.

Taken together, we believe that our results demonstrate the feasibility of conformation-sensitive targeting in general and in IBD in particular. The relationship between conformational state and protein functionality is a commonly seen phenomenon, and targeting specific conformations of proteins opens new avenues in LNP targeting strategies.

However, the integrin conformational change that drives leukocyte extravasation is a complex process. The interaction between receptor and ligand in an activation-dependent manner is enhanced not only by increased affinity but also by increased avidity. Both processes occur naturally and simultaneously to increase ligand-receptor binding, and it is hard to distinguish between the contributions of each of these two processes<sup>34</sup>. To gain more insight into these activation-dependent mechanisms, mAbs have been generated that mimic ligand binding in a conformation-sensitive manner.

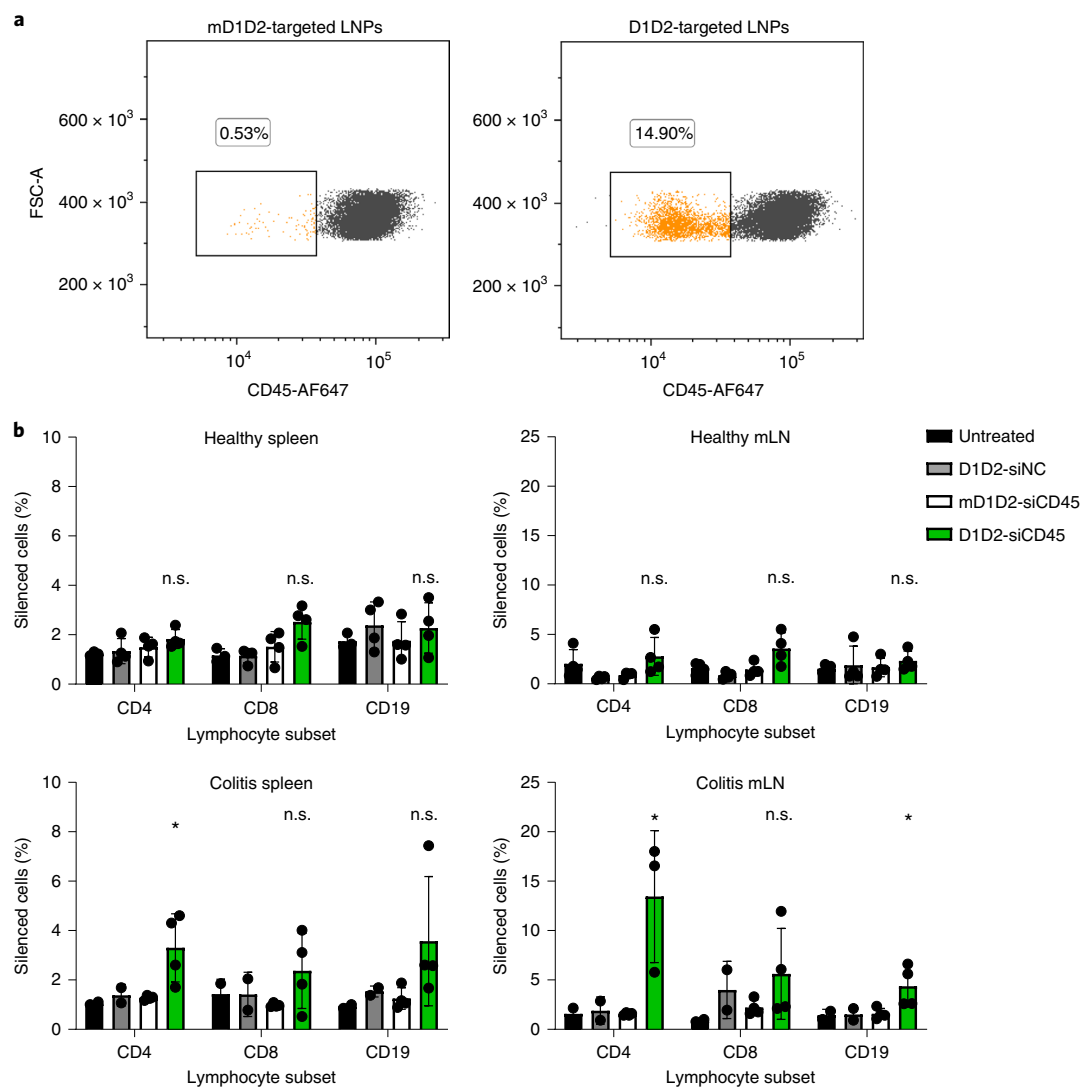


**Fig. 4 | In vivo gene silencing of CD45 using D1D2-targeted LNPs in both healthy mice and mice with colitis.** **a, b**, D1D2 LNPs were either loaded with siRNA against CD45 (siCD45) or with a negative control siRNA (siNC). Untreated mice were used to determine the default CD45 expression levels. Mean fluorescence intensity is shown on both axes. Orange points represent the silenced population, and the percentages indicate the orange points as a percentage of the entire population. **a**, Strongest gene silencing was seen in the CD4<sup>+</sup> T-cell population from the mLN in the PAC model. Observed gene silencing was ~15% as compared to mD1D2 control. **b**, Healthy mice did not show significant silencing in any cell population, while in the PAC model, CD45 was silenced significantly in CD4<sup>+</sup> and CD19<sup>+</sup> cells in the mLNs of colitis-induced mice. Bar height shows the mean; error bars,  $\pm$  s.d.;  $n=5$  mice per group (black points); \*  $P < 0.05$ ; n.s., not significant (statistics performed with two-sided Student's *t*-test comparing D1D2 to mD1D2 for each cell subtype).

For instance, a mAb against a disulfide-locked HA version of LFA-1 was generated to study the role of affinity enhancement in the adhesion process of lymphocytes<sup>34</sup>. Furthermore, an activation-specific mAb that recognizes the HA conformation of the human version of integrin  $\alpha_4\beta_7$  was recently developed using glycan wedges that stabilize the HA conformation<sup>35</sup>. This antibody was generated to study the dynamics of conformational changes and the mechanism of affinity increase.

On a molecular level, much is known about the chemokine-driven, inside-out signalling processes that result in such conformational changes. The conversion of a non-adhesive to an adhesive state of integrins involves extracellular stimuli that activate receptor tyrosine kinases or G protein-coupled receptors, leading to signalling by intracellular integrin binding proteins such as kindlin and talin which in turn induce the conformational change<sup>36,37</sup>.

In vivo, however, the reality is more complex, and little is known about the dynamics. A recombinant mouse model

(C57BL/6-Itgb7<sup>tm1Mshi</sup>/J) with a disrupted  $\alpha_4\beta_7$ -integrin domain leading to a permanent HA conformation<sup>37</sup> can be used to study the conformational changes in greater detail.

As for this study, we have demonstrated that exploiting the conformational changes of an integrin to enhance cell-specific uptake is feasible and that it translates into therapeutic efficacy in experimental colitis. This is a relatively daunting task as it is unknown what percentage of leukocytes display the HA conformation, at which location in the body and for what period of time. Despite the limited knowledge of these in vivo dynamics, we demonstrated the possibility of using HA-integrin- $\alpha_4\beta_7$ -targeted LNPs with a therapeutic payload to produce a therapeutic improvement. In terms of clinical perspective in humans, we envision a novel LNP conjugation strategy without the need for including rat IgG-Fc regions (which could render the protein immunogenic). Such conjugation strategies could include a humanized scFv against a small, non-immunogenic peptide tag that can be integrated into the recombinant protein. If

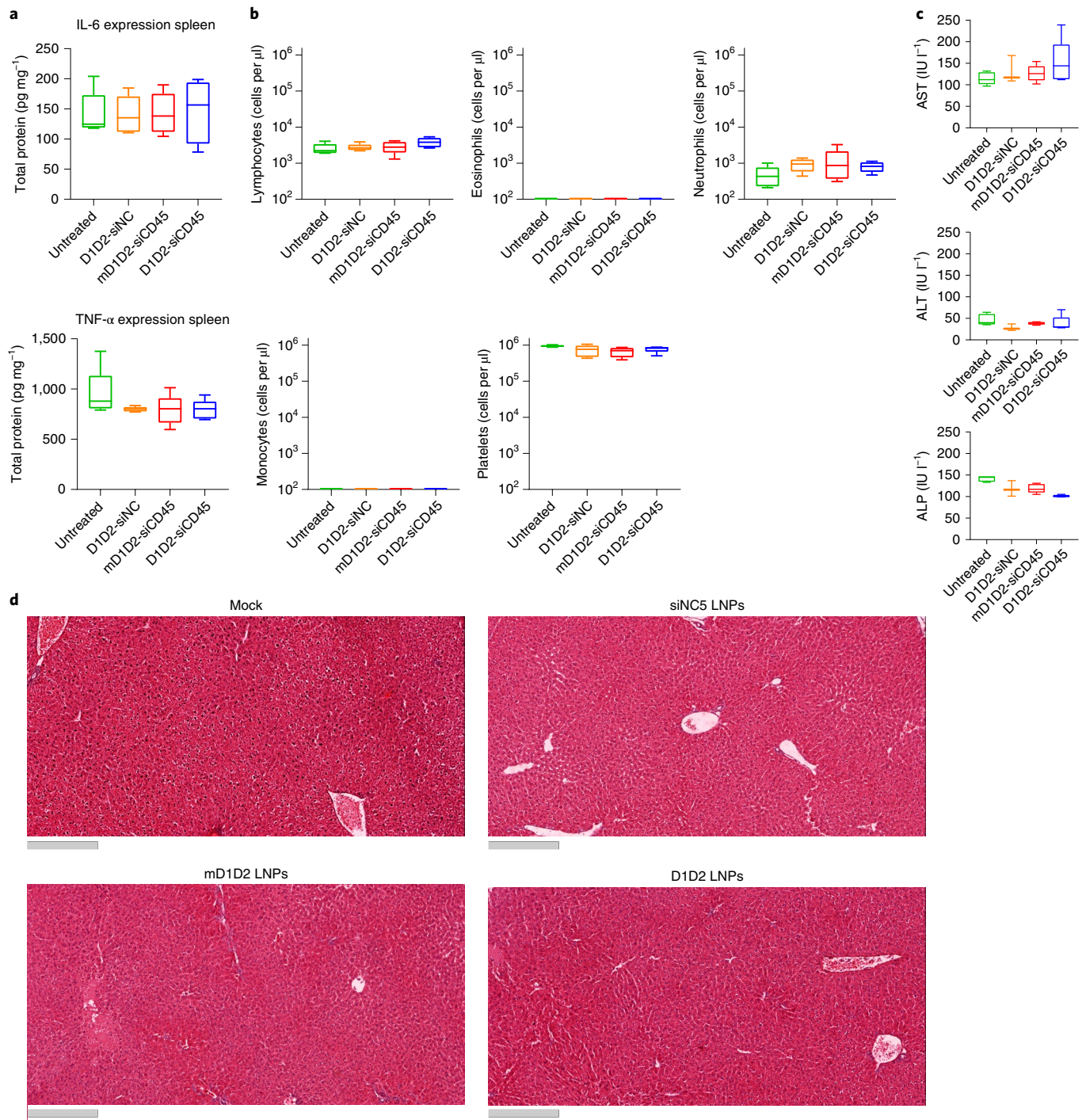


**Fig. 5 | Safety profile of different LNP formulations.** Safety was determined by measuring both liver toxicity and immune activation. **a**, Splenic expression levels of the pro-inflammatory cytokines TNF- $\alpha$  and IL-6. **b**, Complete blood count. **c**, Serum levels of liver enzymes. **d**, Histology of the liver. Scale bar, 300  $\mu$ m. The liver was sectioned and H&E stained. No significant elevation of cytokines, liver enzymes or blood count was detected in the LNP-treated mice compared to the untreated (one-way ANOVA with Dunnett's test comparing each group to the untreated mice,  $n = 5$ ). Liver histology did not reveal tissue damage or excessive bleeding in any of the treated groups. For box plots in **a–c**, the centre of the box shows the median, the bounds of the box show the interquartile range, the lower whisker extends from the lowest value (minimum) to the 25th percentile and the upper whisker extends from the 76th percentile to the highest value (maximum). Experiments were repeated three times independently.

this scFv is lipidated similarly to the ASSET (as described earlier), it will facilitate straightforward incorporation into the LNPs. Another option would be to include an Fc region of a human IgG antibody and chemically conjugate this to the LNPs.

This is a first step demonstrating the feasibility of conformation-sensitive targeting of LNPs for potential future clinical applications. While immunologists discover more defined roles of small subsets of leukocytes, the development of more specific

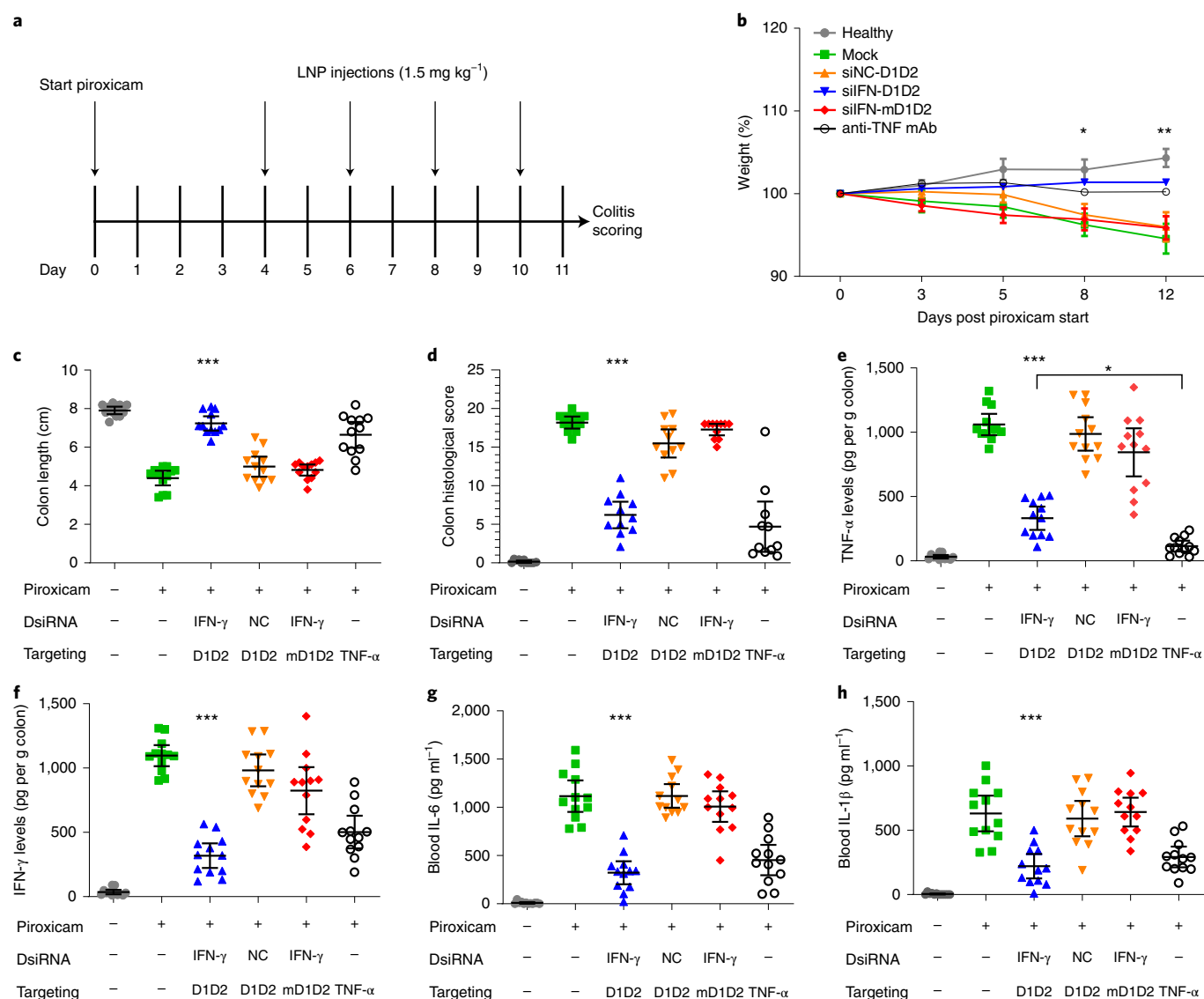


**Fig. 6 | Therapeutic gene silencing of IFN- $\gamma$  using D1D2 LNPs in the PAC model.** **a**, Experimental design. **b**, Percentage weight change in all treated groups with  $n=12$  mice per group. D1D2-silFN showed a significant difference from day 8 onwards. Error bars represent the standard error of the mean. In two groups, the error bars are smaller than the symbols and are therefore not displayed. **c**, Colon length comparison. **d**, Colon histological score index. **e–h**, Expression levels of pro-inflammatory cytokines in the colon (**e–f**) and blood (**g–h**). Data in **c–h** are represented as scatter dot plots with error bars representing the 95% confidence interval. Statistical tests were calculated using one-way ANOVA with Dunnett's post hoc test;  $n=12$  mice per group; \*  $P<0.05$ , \*\*  $P<0.01$ , \*\*\*  $P<0.0001$ . Statistical significance in the plots indicates a difference in the siFN- $\gamma$ -D1D2 LNP group compared to the negative control groups (siFN- $\gamma$ -mD1D2, siNC-D1D2 and untreated mice with colitis). Additionally, **e** indicates a significant difference specifically between the siFN- $\gamma$ -D1D2 and the mAb-TNF- $\alpha$  groups. In the other plots, significant differences between these two groups were absent. Therefore, overall, the therapeutic outcome with D1D2-silFN- $\gamma$  was comparable to the anti-TNF- $\alpha$  mAb. DsiRNA, dicer substrate interfering RNA.

drug delivery systems can accordingly deliver therapeutic payloads to more precisely defined cell populations and revolutionize precision nanomedicine.

### Online content

Any methods, additional references, Nature Research reporting summaries, source data, extended data, supplementary information, acknowledgements, peer review information; details of author contributions and competing interests; and statements of data and code availability are available at <https://doi.org/10.1038/s41565-021-00928-x>.

Received: 27 January 2020; Accepted: 7 May 2021;  
Published online: 17 June 2021

### References

- Elinav, E. & Peer, D. Harnessing nanomedicine for mucosal theranostics—a silver bullet at last? *ACS Nano* **7**, 2883–2890 (2013).
- Hanauer, S. B. et al. Incidence and importance of antibody responses to infliximab after maintenance or episodic treatment in Crohn's disease. *Clin. Gastroenterol. Hepatol.* **2**, 542–553 (2004).
- Baert, F. et al. Influence of immunogenicity on the long-term efficacy of infliximab in Crohn's disease. *N. Engl. J. Med.* **348**, 601–608 (2003).
- Kedmi, R. et al. A modular platform for targeted RNAi therapeutics. *Nat. Nanotechnol.* **13**, 214–219 (2018).
- Veiga, N. et al. Cell specific delivery of modified mRNA expressing therapeutic proteins to leukocytes. *Nat. Commun.* **9**, 4493 (2018).
- Whitehead, K. A., Langer, R. & Anderson, D. G. Knocking down barriers: advances in siRNA delivery. *Nat. Rev. Drug Discov.* **8**, 129–138 (2009).
- Fenske, D. B., Chonn, A. & Cullis, P. R. Liposomal nanomedicines: an emerging field. *Toxicol. Pathol.* **36**, 21–29 (2008).

8. Ledford, H. Gene silencing technology gets first drug approval after 20-year wait. *Nature* **560**, 291–292 (2018).
9. Ramishetti, S. et al. Systemic gene silencing in primary T lymphocytes using targeted lipid nanoparticles. *ACS Nano* **9**, 6706–6716 (2015).
10. Peer, D., Park, E. J., Morishita, Y., Carman, C. V. & Shimaoka, M. Systemic leukocyte-directed siRNA delivery revealing cyclin D1 as an anti-inflammatory target. *Science* **319**, 627–630 (2008).
11. Meenan, J. et al. Altered expression of  $\alpha 4\beta 7$ , a gut homing integrin, by circulating and mucosal T cells in colonic mucosal inflammation. *Gut* **40**, 241–246 (1997).
12. Yu, Y. et al. Structural specializations of  $\alpha 4\beta 7$ , an integrin that mediates rolling adhesion. *J. Cell Biol.* **196**, 131–146 (2012).
13. Sun, H. et al. Distinct chemokine signaling regulates integrin ligand specificity to dictate tissue-specific lymphocyte homing. *Dev. Cell* **30**, 61–70 (2014).
14. Lichtenstein, G. R., Hanauer, S. B. & Sandborn, W. J. Risk of biologic therapy-associated progressive multifocal leukoencephalopathy: use of the JC virus antibody assay in the treatment of moderate-to-severe Crohn's disease. *Gastroenterol. Hepatol.* **8**, 1–20 (2012).
15. Green, N. et al. Mutational analysis of MAdCAM-1/ $\alpha 4\beta 7$  interactions reveals significant binding determinants in both the first and second immunoglobulin domains. *Cell Adhes. Commun.* **7**, 167–181 (1999).
16. Shyjan, A. M., Bertagnolli, M., Kenney, C. J. & Briskin, M. J. Human mucosal addressin cell adhesion molecule-1 (MAdCAM-1) demonstrates structural and functional similarities to the  $\alpha 4\beta 7$ -integrin binding domains of murine MAdCAM-1, but extreme divergence of mucin-like sequences. *J. Immunol.* **156**, 2851–2857 (1996).
17. Berlin, C. et al.  $\alpha 4\beta 7$  integrin mediates lymphocyte binding to the mucosal vascular addressin MAdCAM-1. *Cell* **74**, 185–195 (1993).
18. Dearling, J. L. J. et al. Detection of intestinal inflammation by MicroPET imaging using a  $^{64}\text{Cu}$ -labeled anti- $\beta 7$  integrin antibody. *Inflamm. Bowel Dis.* **16**, 1458–1466 (2010).
19. Dearling, J. L. J., Daka, A., Veiga, N., Peer, D. & Packard, A. B. Colitis immunoPET: defining target cell populations and optimizing pharmacokinetics. *Inflamm. Bowel Dis.* **22**, 529–538 (2016).
20. Belliveau, N. M. et al. Microfluidic synthesis of highly potent limit-size lipid nanoparticles for in vivo delivery of siRNA. *Mol. Ther. Nucleic Acids* **1**, e37 (2012).
21. Cohen, Z. R. et al. Localized RNAi therapeutics of chemoresistant grade IV glioma using hyaluronan-grafted lipid-based nanoparticles. *ACS Nano* **9**, 1581–1591 (2015).
22. Veiga, N. et al. Leukocyte-specific siRNA delivery revealing IRF8 as a potential anti-inflammatory target. *J. Control Release* **313**, 33–41 (2019).
23. Rosenblum, D., Joshi, N., Tao, W., Karp, J. M. & Peer, D. Progress and challenges towards targeted delivery of cancer therapeutics. *Nat. Commun.* **9**, 1410 (2018).
24. Chassaing, B., Aitken, J. D., Malleshappa, M. & Vijay-Kumar, M. Dextran sulfate sodium (DSS)-induced colitis in mice. *Curr. Protoc. Immunol.* **104**, 15.25.1–15.25.14 (2014).
25. Dieleman, L. A. et al. Dextran sulfate sodium-induced colitis occurs in severe combined immunodeficient mice. *Gastroenterology* **107**, 1643–1652 (1994).
26. Berg, D. J. et al. Rapid development of colitis in NSAID-treated IL-10 deficient mice. *Gastroenterology* **123**, 1527–1542 (2002).
27. Holgersen, K., Kvist, P. H., Markholst, H., Kornerup Hansen, A. & Holm, T. L. Characterisation of enterocolitis in the piroxicam-accelerated interleukin-10 knock out mouse—a model mimicking inflammatory bowel disease *J. Crohn's Colitis* **8**, 147–160 (2012).
28. Holgersen, K., Kvist, P. H., Hansen, A. K. & Holm, T. L. Predictive validity and immune cell involvement in the pathogenesis of piroxicam-accelerated colitis in interleukin-10 knockout mice. *Int. Immunopharmacol.* **21**, 137–147 (2014).
29. Connor, E. M., Eppihimer, M. J., Morise, Z., Granger, D. N. & Grisham, M. B. Expression of mucosal addressin cell adhesion molecule-1 (MAdCAM-1) in acute and chronic inflammation. *J. Leukoc. Biol.* **65**, 349–355 (1999).
30. Ito, R. et al. Interferon- $\gamma$  is causatively involved in experimental inflammatory bowel disease in mice. *Clin. Exp. Immunol.* **146**, 330–338 (2006).
31. Ferreira, R. & Barreiro-de Acosta, M. *Infliximab: Pharmacology, Uses and Limitations* 1st edn (eds Acevedo, A. D. M. & Gaitan, M. F.) 39–74 (Nova Biomedical, 2012).
32. Vila-del Sol, V., Punzón, C. & Fresno, M. IFN- $\gamma$ -induced TNF- $\alpha$  expression is regulated by interferon regulatory factors 1 and 8 in mouse macrophages. *J. Immunol.* **181**, 4461–4470 (2008).
33. Wesemann, D. R. & Benveniste, E. N. STAT-1 $\alpha$  and IFN- $\gamma$  as modulators of TNF- $\alpha$  signaling in macrophages: regulation and functional implications of the TNF receptor 1:STAT-1 $\alpha$  complex. *J. Immunol.* **171**, 5313–5319 (2003).
34. Shimaoka, M. et al. AL-57, a ligand-mimetic antibody to integrin LFA-1, reveals chemokine-induced affinity up-regulation in lymphocytes. *Proc. Natl Acad. Sci. USA* **103**, 13991–13996 (2006).
35. Qi, J. P. et al. Identification, characterization, and epitope mapping of human monoclonal antibody J19 that specifically recognizes activated integrin  $\alpha 4\beta 7$ . *J. Biol. Chem.* **287**, 15749–15759 (2012).
36. Kinashi, T. Intracellular signalling controlling integrin activation in lymphocytes. *Nat. Rev. Immunol.* **5**, 546–559 (2005).
37. Eun, J. P. et al. Aberrant activation of integrin  $\alpha 4\beta 7$  suppresses lymphocyte migration to the gut. *J. Clin. Invest.* **117**, 2526–2538 (2007).

**Publisher's note** Springer Nature remains neutral with regard to jurisdictional claims in published maps and institutional affiliations.

© The Author(s), under exclusive licence to Springer Nature Limited 2021

## Methods

### Antibodies.

Rat anti-mouse  $\alpha_4\beta_7$  integrin (Clone DATK32, Biologend)  
 Rat anti-mouse  $\beta_7$  integrin (Clone FIB504, BioXCell)  
 Mouse anti-rat IgG<sub>2a</sub> (Clone RG7/1.30, BioXCell)  
 Rat IgG<sub>2a</sub> isotype control (Clone 2A3, BioXCell)  
 PE-conjugated donkey anti-mouse IgG (Polyclonal, Jackson Immuno Research)  
 Alexa Fluor 647-conjugated goat anti-rat IgG (Polyclonal, Biologend)  
 Alexa Fluor 647-conjugated mouse anti-human IgG (Polyclonal, Biologend)  
 Alexa Fluor 647-conjugated rat anti-mouse CD45 (Clone 30-F11, Biologend)  
 Alexa Fluor 488-conjugated rat anti-mouse CD45 (Clone 30-F11, Biologend)  
 BV650-conjugated rat anti-mouse/human CD11b (Clone M1/70, Biologend)  
 PE/Cy5-conjugated rat anti-mouse CD19 (Clone 6D5, Biologend)  
 BV421-conjugated hamster anti-mouse CD3e (Clone 145-2C11, Biologend)  
 APC/Cy7-conjugated rat anti-mouse CD4 (Clone GK1.5, Biologend)  
 Alexa Fluor 488-conjugated rat anti-mouse CD8a (Clone 53-6.7, Biologend)  
 PE-conjugated rat anti-mouse CD8a (Clone 53-6.7, Biologend)  
 PE/Dazzle 594 rat anti-mouse CD25 (Clone PC61, Biologend)  
 BV510 Armenian hamster anti-mouse CD69 (Clone H1.2F3, Biologend)  
 PE-conjugated rat anti-mouse FOXP3 (Clone MF-14, Biologend)  
 Horseradish peroxidase (HRP)-conjugated donkey anti-rat IgG (Polyclonal, Jackson Immuno Research)

**siRNAs.** The siRNA against CD45 and the corresponding negative control siRNA are chemically modified siRNAs and were kindly provided as a gift by Alnylam Pharmaceuticals.

The siRNA against IFN- $\gamma$  and the corresponding negative control siRNA are chemically modified dicer substrates (synthesized by Integrated DNA Technologies).

### Mouse CD45 siRNA. Sense:

mCmUrGrGmCmUrGrArAmUmUmCrArGrArGmCrAdTsdT  
 Antisense: rUrGrCrUrCrUrGrArArArUrUmCrArGrCmCrArGdTsdT

### Negative control siRNA. Sense:

mCmUmUmCrGmCmUrGrArGmUrAmCmUmUmCrGAdTsdT  
 Antisense: rUrCrGrArArGmUrArCrUmCrArGrCrGmUrArArGdTsdT

### Mouse IFN- $\gamma$ dicer substrate. Sense:

mCmArUmUrCmArUrGrArGrUmArUmUrGmCrCmArArGrUrUrUmGm  
 Antisense:  
 rUrCmArArArCrUrUmGrGmCrAmArUrArCrUrCrArUrGrAmArUmGmCm

### Negative control dicer substrate. Sense:

mCmArUmArUmUrGrCrGrCrGmUrAmUrAmGrUmCrGrCrUrUmAG  
 Antisense:  
 rCrUmArArCrGrGmArCmUrAmUrArCrGrCrGrCrArArUmArUmGmGmU  
 where 'm' is 2'-OMe-modified nucleotides, 'r' is RNA bases (nucleotides without 'r' or 'm' represent DNA bases) and 's' is phosphorothioate linkage.

**Cloning.** Sequences of the primers are listed in Supplementary Fig. 10. Murine MAdCAM-1-D1D2 was synthesized as a gBlock gene fragment (Integrated DNA Technologies) and complementary DNA of rat IgG<sub>2a</sub> was obtained from an in-house hybridoma clone using RNeasy minikit (Qiagen) and qScript cDNA synthesis kit (Quantabio). The Fc of rat IgG<sub>2a</sub> was amplified from the obtained cDNA using primer pair F1 and R1; the primers added the required homology sequences for the Gibson assembly to the 5' ends of the amplicon. Next, the murine MAdCAM-D1D2 and IgG-Fc were assembled in the pCMV3-FLAG plasmid using Gibson assembly (New England Biolabs). In a later stage, the entire construct was reassembled in the pcDNA3.4 expression plasmid to improve protein yields using primer pair F2 and R2. The point mutation for the negative control was generated using site-directed mutagenesis; primers F3 and R3 amplified the entire plasmid while generating the point mutation. The resulting PCR product was DpnI digested, purified on a 0.8% agarose gel, phosphorylated using T4 polynucleotide kinase (New England Biolabs), circularized using T4 DNA ligase (New England Biolabs) and transformed into chemically competent bacteria. To improve flexibility in the context of the LNPs, the C<sub>H1</sub> domain of rat IgG<sub>2a</sub> was later removed by PCR amplification of the entire plasmid using primers F4 and R4. See Supplementary Fig. 10 for the sequence of the entire construct.

**Cell culture.** Cell lines used were Expi293 (ThermoFisher Scientific), TK-1 (ATCC) and HEK293 (ATCC). All cell lines in the laboratory were tested every two months for mycoplasma and discarded when positive. Expi293 cells were grown in Expi293 expression medium (ThermoFisher Scientific) in disposable Erlenmeyer flasks at 37°C and 8% CO<sub>2</sub> on a shaker rotating at 125 r.p.m. Cells were grown at densities between  $0.3 \times 10^6$  and  $5 \times 10^6$  cells per ml. At least three passages after thawing, cells were transfected with the expression plasmid encoding the MAdCAM-D1D2-Fc using the ExpiFectamine293 transfection kit (ThermoFisher Scientific). Eighteen hours post transfection, enhancer 1 and enhancer 2 from the ExpiFectamine293 transfection kit were added to boost recombinant protein

expression levels. Five days post transfection, the culture medium was harvested for purification of the secreted protein.

TK-1 cells were grown in RPMI1640 medium supplemented with 10% fetal bovine serum, L-glutamine and Pen-Strep-Nystatin (Biological Industries). Cells were grown at densities between  $0.3 \times 10^6$  and  $2 \times 10^6$  cells per ml in either T25 or T75 cell culture flasks (Greiner Bio-One).

**Protein purification.** Conditioned medium was separated from the Expi293 cells by centrifugation at 300g for 5 min. The supernatant was centrifuged again at 5,000g for 20 min to remove cellular debris. Using the Äkta FPLC protein purification system (GE Healthcare), the protein was purified with a 1 ml HisTrap column (GE Healthcare). The sample was adjusted to the composition of the binding buffer (20 mM NaPO<sub>4</sub> at pH 7.4 and 500 mM NaCl), and the sample was passed through a 0.2  $\mu$ m syringe filter (Sartorius) before loading into the FPLC. Flow rate during binding and elution was 0.5 ml min<sup>-1</sup>, and during washes, 1 ml min<sup>-1</sup>. The columns were washed with 20 ml of 0.5 M NaOH and 20 ml deionized water before being equilibrated with 10 ml of binding buffer and loaded with the sample. Protein elution was done using binding buffer supplemented with 0.5 M imidazole. The elution was performed stepwise with incremental increases of ~30 mM imidazole per fraction until the final concentration of 0.5 M was reached. Fractions were loaded on SDS-PAGE gel and stained with Coomassie to determine which fractions contained the MAdCAM-Fc at sufficient purity. Pooled fractions were buffer-exchanged to PBS using PD-10 desalting columns (GE Healthcare). The purified protein was concentrated to  $>1$  mg ml<sup>-1</sup> using Amicon ultra centrifugal filters (EMD Millipore), snap-frozen in liquid nitrogen and stored at -80°C.

**SDS-PAGE gel analysis.** Protein samples were diluted in sample buffer with or without the presence of 500 mM dithiothreitol to compare between monomers and dimers (presence of the hinge domain should dimerize the D1D2). Samples were loaded on a 10% polyacrylamide gel and either stained with Coomassie (Bio-rad) or transferred to a nitrocellulose membrane using iBlot 2 dry blotting system (ThermoFisher Scientific). Membranes were blocked with 5% skim milk in PBS for 2 h at room temperature and incubated with anti-rat IgG-HRP. Membranes were washed with PBS + 0.01% Tween20 and developed using SuperSignal West Pico chemiluminescent substrate (ThermoFisher Scientific). Chemiluminescence was measured with the Amersham Imager 600 (GE Healthcare).

**In vitro binding.** TK-1 cells were activated according to Yang et al.<sup>38</sup> Briefly, cells were washed with PBS and resuspended in resuspension buffer (HBSS with 10 mM HEPES buffer, 2 mM CaCl<sub>2</sub> and 2 mM MgCl<sub>2</sub>). Non-activated cells were kept on ice while activated cells were resuspended in pre-incubation buffer (HBSS with 10 mM HEPES buffer and 2 mM EDTA), incubated at room temperature for 30 min with gentle rotation, washed with PBS and finally resuspended in activation buffer (HBSS with 10 mM HEPES buffer, 2 mM CaCl<sub>2</sub> and 2 mM MnCl<sub>2</sub>). MAdCAM-Fc and the controls were added to both activated and non-activated cells and incubated for 30 min at 4°C. Cells were subsequently washed and stained with either anti-human IgG or anti-mouse IgG conjugated to Alexa Fluor 647. Binding of MAdCAM to TK-1 cells was assessed by analysing the fluorescence of the cells by flow cytometry. Binding of MAdCAM-targeted Cy5 LNPs was detected by flow cytometry directly using the Cy5 fluorescence (without addition of another antibody). Because of a higher background using LNPs, in binding experiments with Cy5 LNPs, the HBSS in the activation buffer was replaced with RPMI + 10% FBS.

**Preparation of LNPs.** LNPs were prepared as previously described<sup>39</sup> by using the NanoAssemblr microfluidic mixer (Precision Nanosystems). Here, we utilized the current gold standard for LNP production, DLin-MC3-DMA, an ionizable lipid with a pK<sub>a</sub> of 6.44 that has a positive charge under acidic conditions. LNPs were prepared at pH 4.5 to ensure that DLin-MC3-DMA is ionized and hence siRNA encapsulation is maximized. Lipid mixture (Dlin-MC3-DMA, DSPC, cholesterol, PEG-DMG and DSPE-PEG-maleimide at a 50:10:38:1.5:0.5 molar ratio) in ethanol was mixed with siRNA in acetate buffer, pH 4.5, at a combined flow rate of 2 ml min<sup>-1</sup>. Lipid and siRNA were mixed at a 1:3 volume ratio (1:16 w/w siRNA to lipid). For Cy5-labelled LNPs, 20% Cy5-labelled siRNA was mixed with 80% unlabelled siRNA. The resulting LNPs were dialysed against PBS for 24 h to remove the ethanol and restore the pH to neutral. The hydrodynamic diameter and zeta potential of the LNPs were measured by dynamic light scattering using disposable cuvettes in the Malvern Zetasizer (Malvern Instruments).

**Determining the siRNA encapsulation efficiency.** LNPs were either lysed with Triton X-100 or not and the total amount of siRNA in the sample was measured with the Quant-iT Ribogreen RNA assay kit (ThermoFisher Scientific). After subtracting the blank measurement, the encapsulation efficiency (in percentage) was calculated as  $(1 - (\text{non-lysed LNPs} / \text{lysed LNPs})) \times 100$ .

**Conjugation of RG7 to LNPs and gel filtration.** RG7/1.3 antibody was reduced in PBS supplemented with 1 mM dithiothreitol and 5 mM EDTA by incubating 1 h at room temperature. The dithiothreitol was subsequently removed by buffer exchange to 5 mM EDTA in PBS using 7K Zeba Spin Desalting Columns (ThermoFisher Scientific). Immediately after buffer exchange, the reduced antibody was added

to the LNPs at a ratio of 0.67 mg antibody per ml of LNPs. The mixture was incubated for 2 h at room temperature with gentle shaking followed by overnight incubation at 4 °C. The next day, LNPs were separated from the free antibody using sepharose CL4B beads on a gel filtration column with PBS as the mobile phase. Fractions containing pure LNPs were pooled and concentrated to the initial volume using 100K Amicon centrifugal filters (EMD Millipore). The loss of LNPs during conjugation and gel filtration was estimated by lysing LNPs before and after conjugation with Triton X-100 followed by measuring the amount of released siRNA using a Quant-iT Ribogreen RNA assay kit (ThermoFisher Scientific).

**Dot-blot analysis.** Dot-blot analysis was performed using Minifold I system 96-well device (GE Healthcare). A nitrocellulose membrane was added on top of two filter papers (Whatman plc) and loaded into the 96-well dot-blot device. Wells were filled with PBS and vacuum was applied to wet the membrane. Samples (conjugated LNPs, unconjugated LNPs and several different amounts of free antibody) were added to the wells in a 100 µl volume followed by a vacuum to pass the sample through the membrane. Wells were washed with PBS and the device was again applied to a vacuum. Next, the membrane was blocked with 5% skim milk in PBS for 2 h followed by incubation with anti-mouse IgG antibody linked to HRP (diluted in PBS with 1% skim milk) for 1 h at room temperature. Next, the membrane was washed three times with PBST (5 min per wash) and the samples were detected by adding the SuperSignal West Pico chemiluminescent substrate (ThermoFisher Scientific). Chemiluminescence was measured with the Amersham Imager 600 (GE Healthcare).

**Confocal microscopy.** Cells were stained with Hoechst (nucleus) and with Alexa Fluor 488-conjugated anti-CD45 (cell membrane). Cells were resuspended in PBS and images were taken with a Zeiss confocal microscope. The images were created by merging 11 frames from a z-stack with 0.3 µm per frame.

**Ex vivo binding.** Leukocytes were extracted from the spleen and mLN of both healthy C57Bl/6 mice and IL-10KO mice that spontaneously developed colitis. For the mLN, tissue was homogenized and cells were strained through a 70 µm cell strainer. Cells were washed with PBS and centrifuged before the pellet was washed again with PBS and resuspended as a single-cell suspension. For the spleen, tissue was homogenized and cells were strained through a 70 µm cell strainer. After a single wash with PBS, red blood cells were lysed with ddH<sub>2</sub>O for a few seconds followed by addition of 10x HBSS to restore the solution to physiological conditions. Cells were strained a second time to ensure a single-cell suspension. Next, cells were stained with the appropriate cell surface markers (CD4, CD8, CD19 or CD11b) and allowed to bind to either D1D2 LNPs or DATK32 LNPs (or their respective controls, mD1D2 LNPs and isotype LNPs). After a 20 min incubation at 4 °C, cells were washed and resuspended in FACS buffer. LNP binding for each leukocyte subpopulation was determined by the level of Cy5 as measured by flow cytometry.

**Animal experiments.** The Tel Aviv Institutional Animal Care and Use Committee approved the animal protocols for all in vivo studies in accordance with current regulations and standards of the Israel Ministry of Health.

**In vivo gene silencing.** Wild-type C57Bl/6 and IL-10KO C57Bl/6 mice were kept in a specific-pathogen-free animal facility at Tel Aviv University. For the DSS colitis model, DSS was added to the drinking water at a concentration of 1.5% for a total of 10 days. Five days after DSS administration, LNPs were injected intravenously and CD45 expression in various organs was assessed 5 days post injection. For the PAC colitis model, piroxicam was administered to IL-10KO mice in the chow at a concentration of 200 ppm for a total of 11 days. Seven days after administration of piroxicam, LNPs were injected and CD45 expression in various organs was assessed 4 days post injection. For healthy mice, CD45 expression was assessed 4 days post injection. After euthanizing the animals, organs were homogenized, and single-cell suspensions were obtained using 70 µm cell strainers (Corning). Cells were stained with antibodies against CD3 (Brilliant Violet 421), CD4 (APC-Cy7), CD8a (Alexa Fluor 488), CD19 (PE-Cy5.5), CD11b (Brilliant Violet 650), F4/80 (Brilliant Violet 605) and CD45 (Alexa Fluor 647) and analysed by flow cytometry.

**In vivo safety study.** Female, ten-week-old C57Bl/6 mice (Harlan laboratories) were injected with LNPs at a dose of 1.5 mg kg<sup>-1</sup> and killed 24 h later. Blood was collected and analysed by AML Israel for complete blood count (Sysmex and Advida-120) and biochemistry (Cobas-6000). Liver samples were used for histology (Histospeck). Splenic TNF-α and IL-6 levels were measured by DuoSet ELISA kits (R&D Systems).

**Therapeutic efficacy studies with siIFN-γ.** To test in silico optimized siRNA sequences against murine IFN-γ, HEK293 cells stably expressing murine IFN-γ were generated by transfecting the cells with a pcDNA3 plasmid harbouring the murine IFN-γ gene. Stably expressing cells were selected with G418. Next, cells were transfected with each of the siRNA sequences and with a control sequence (siNC). Forty-eight hours post transfection, cells were lysed, RNA was extracted and cDNA was generated. Silencing efficiency was determined using quantitative

PCR with SYBR green. The sequence that most efficiently silenced IFN-γ was used for the subsequent efficacy experiments.

For the efficacy studies, colitis was induced in nine-week-old female C57Bl/6 IL-10KO mice by mixing piroxicam (200 ppm) in the food. Freshly prepared LNPs (encapsulated with either siIFN-γ or siNC) were conjugated to RG7 and purified using CL4B resin. LNPs were injected intravenously at days 4, 6, 8 and 10 post piroxicam administration. The volume of administered LNPs was calculated with the Ribogreen assay (ThermoFisher Scientific) for each LNP preparation to ensure a consistent dose of 1.5 mg siRNA per kg body weight. Thirty minutes prior to injection, LNPs were mixed with the D1D2 or mD1D2 (final protein concentration of 60 µg ml<sup>-1</sup>) and the total volume was completed to 200 µl.

Animals were randomized before piroxicam treatment, and the study was performed in a double-blinded fashion. The experiment was performed by a contract research organization to ensure that the investigator was blinded during group allocation.

Body weight was recorded daily, and at day 11 of the experiment the mice were killed. The colon was harvested to measure the length, to analyse colonic cytokine levels and to perform colon histology. Blood samples were collected to measure IL-6 and IL-1β expression levels.

**Molecular imaging studies.** 1,4,7-Triazacyclononane-1,4-bis-acetic acid-7-maleimidoethylacetamide (NOTA-mal, Macrocylics) was conjugated to the immunoprotein using a previously described approach with minor modifications<sup>40</sup>. Briefly, to 500 µg of protein in 150 µl of phosphate buffer (pH 7.0) was added freshly prepared 2-iminothiolane and then NOTA-mal in phosphate buffer (10% dimethylsulfoxide) and 2IT such that final concentration ratios were as follows: Ab, 1; NOTA-mal, 20 and 2IT, 10. The reaction was mixed by gentle pipetting, briefly centrifuged, and then placed in a 37 °C water bath for 30 min. Unbound chelator was removed using centrifugal filter units (3 kDa MW cut-off; Centricon, Millipore), and the immunoconjugate was concentrated into phosphate buffer (0.1 M, pH 7.0) and stored in aliquots at -80 °C.

For the radiolabelling, six volume equivalents of sodium acetate buffer were added to 178 MBq (4.78 mCi) <sup>64</sup>Cu in 5 µl HCl (0.04 N). Antibody (177 µg in 61 µl phosphate buffer) was then added to 15.8 µl of <sup>64</sup>Cu solution (31.7 MBq (858 µCi)). After 30 min incubation at room temperature, the degree of radiolabelling was assessed by thin-layer chromatography (Whatman No.1 paper eluted with phosphate buffer; 0.1 M, pH 8, 100 mM EDTA) and radiochemical purity was found to be >95%. The radioimmunoconjugate was diluted with saline and sterile filtered (0.2 µm) before injection.

For the imaging studies, <sup>64</sup>Cu-labelled antibody (22 µg antibody, 3.12 MBq (84.3 µCi)) was injected into the tail vein. The mice were then anaesthetized using isoflurane (1–4% in oxygen) and placed in a Bruker Albira multimodality (PET/CT) small-animal imaging system (Bruker) for imaging. PET/CT data were collected for 30 min at 1, 3 and 24 h post injection. At 24 h post injection, the mice were euthanized by CO<sub>2</sub> inhalation, and an ex vivo biodistribution analysis was carried out. Tissues were collected and weighed, and the radioactivity was assayed. The large colon was excised, measured and weighed to confirm the presence of colitis in the piroxicam-treated group. PET and CT images were registered manually using AMIDE software<sup>41</sup>. Data from volumes of interest were used to calculate the biodistribution in selected tissues for the small-animal PET imaging studies.

**Statistical analysis.** Data in the bar charts are expressed as mean ± standard deviation unless otherwise indicated. In box plots, the centre line represents the median, the box represents the interquartile range and the whiskers represent minimum and maximum values. Statistical analysis was performed in GraphPad Prism. In general, when comparing two groups (for instance, mD1D2 to D1D2), Student's *t*-test was used, and a one-way ANOVA was used when comparing three or more groups. A more complex statistical model (two-way interaction mixed model) was used in the molecular imaging section to confirm the correlation between colitis severity and D1D2 uptake, and this is shown in Supplementary Fig. 6.

More specifically, for the CD45 silencing, a two-sided Student's *t*-test was performed between the groups mD1D2 and D1D2. For the toxicity study, a one-way ANOVA test was performed to exclude significant differences between any of the groups. For the efficacy study, a one-way ANOVA with Dunnett's post hoc test was used to demonstrate a significant difference between the D1D2-IFN-γ group and the negative control groups (D1D2-NC5, mD1D2-IFN-γ and mock-treated). The same post hoc test revealed a significant difference between the groups D1D2-IFN-γ and mAb-TNF-α only in the colonic TNF-α expression levels (*P* < 0.05). Group size for the in vivo silencing and toxicity study was five mice per group. In the efficacy study, group size was increased to 12 mice per group due to relatively high standard deviations in smaller group sizes. In all figures, \* stands for *P* < 0.05, \*\* for *P* < 0.01 and \*\*\* for *P* < 0.0001.

**Reporting Summary.** Further information on research design is available in the Nature Research Reporting Summary linked to this article.

## Data availability

All relevant data are available from the authors upon reasonable request.

## References

38. YANG, Y. et al. Construction and adhesive properties of a soluble MAdCAM-1–Fc chimera expressed in a baculovirus system: phylogenetic conservation of receptor–ligand interaction. *Scand. J. Immunol.* **42**, 235–247 (1995).
39. Rungta, R. L. et al. Lipid nanoparticle delivery of siRNA to silence neuronal gene expression in the brain. *Mol. Ther. Nucleic Acids* **2**, e136 (2013).
40. McCall, M. J., Diril, H. & Meares, C. F. Simplified method for conjugating macrocyclic bifunctional chelating agents to antibodies via 2-iminothiolane. *Bioconjugate Chem.* **1**, 222–226 (1990).
41. Loening, A. M. & Gambhir, S. S. AMIDE: a free software tool for multimodality medical image analysis. *Mol. Imaging* **2**, 131–137 (2003).

## Acknowledgements

We thank V. Holdengreber for assistance with the transmission electron microscopy analysis, P. Johnston for detailed statistical analysis of the molecular imaging part, S. Chatterjee for help with the confocal microscope and S. Jung for providing the IL-10KO mice. This work was supported by the ERC grant LeukoTheranostics (award no. 647410) to D.P.

## Author contributions

N.D. and D.P. conceived the study. N.D., S.R., N.V., M.G. and J.L.J.D. performed the experiments. N.D., J.L.J.D., A.B.P., M.G. and D.P. analysed the data. N.D. and D.P. wrote the manuscript.

## Competing interests

D.P. receives licensing fees (to patents on which he was an inventor) from, invested in, consults (or on scientific advisory boards or boards of directors) for, lectured (and received a fee) or conducts sponsored research at TAU for the following entities: Alnylam Pharmaceuticals Inc. Arix Biosciences Inc., ART Biosciences, BioNtech RNA pharmaceuticals; Centricus, Diagnostear Ltd., EPM Inc., Earli Inc., Impetis Biosciences, Kernal Biologics, GPCR Inc., Medison Pharma Ltd., Newphase Ltd, NLC Pharma Ltd., Nanocell Therapeutics, NanoGhosts Ltd., Precision Nanosystems Inc., Paul Hastings Inc., Regulon, Roche, SciCann, Shire Inc., VLX Ventures, TATA Cooperation, Teva Pharmaceuticals Inc., Wize Pharma Ltd. All other authors declare no competing financial interests. None of them relates to this work. The rest of the authors declare no financial interests.

## Additional information

**Supplementary information** The online version contains supplementary material available at <https://doi.org/10.1038/s41565-021-00928-x>.

**Correspondence and requests for materials** should be addressed to D.P.

**Peer review information** *Nature Nanotechnology* thanks Monica Baiula, JianFeng Chen, Yizhou Dong and the other, anonymous, reviewer(s) for their contribution to the peer review of this work.

**Reprints and permissions information** is available at [www.nature.com/reprints](http://www.nature.com/reprints).

## Reporting Summary

Nature Research wishes to improve the reproducibility of the work that we publish. This form provides structure for consistency and transparency in reporting. For further information on Nature Research policies, see our [Editorial Policies](#) and the [Editorial Policy Checklist](#).

### Statistics

For all statistical analyses, confirm that the following items are present in the figure legend, table legend, main text, or Methods section.

- | n/a                                 | Confirmed  |
|-------------------------------------|--|
| <input type="checkbox"/>            | <input checked="" type="checkbox"/> The exact sample size ( $n$ ) for each experimental group/condition, given as a discrete number and unit of measurement  |
| <input type="checkbox"/>            | <input checked="" type="checkbox"/> A statement on whether measurements were taken from distinct samples or whether the same sample was measured repeatedly  |
| <input type="checkbox"/>            | <input checked="" type="checkbox"/> The statistical test(s) used AND whether they are one- or two-sided<br><i>Only common tests should be described solely by name; describe more complex techniques in the Methods section.</i>   |
| <input checked="" type="checkbox"/> | <input type="checkbox"/> A description of all covariates tested  |
| <input checked="" type="checkbox"/> | <input type="checkbox"/> A description of any assumptions or corrections, such as tests of normality and adjustment for multiple comparisons   |
| <input type="checkbox"/>            | <input checked="" type="checkbox"/> A full description of the statistical parameters including central tendency (e.g. means) or other basic estimates (e.g. regression coefficient) AND variation (e.g. standard deviation) or associated estimates of uncertainty (e.g. confidence intervals) |
| <input type="checkbox"/>            | <input checked="" type="checkbox"/> For null hypothesis testing, the test statistic (e.g. $F$ , $t$ , $r$ ) with confidence intervals, effect sizes, degrees of freedom and $P$ value noted<br><i>Give <math>P</math> values as exact values whenever suitable.</i>                            |
| <input checked="" type="checkbox"/> | <input type="checkbox"/> For Bayesian analysis, information on the choice of priors and Markov chain Monte Carlo settings  |
| <input checked="" type="checkbox"/> | <input type="checkbox"/> For hierarchical and complex designs, identification of the appropriate level for tests and full reporting of outcomes  |
| <input checked="" type="checkbox"/> | <input type="checkbox"/> Estimates of effect sizes (e.g. Cohen's $d$ , Pearson's $r$ ), indicating how they were calculated  |

*Our web collection on [statistics for biologists](#) contains articles on many of the points above.*

### Software and code

Policy information about [availability of computer code](#)

Data collection

Data analysis

For manuscripts utilizing custom algorithms or software that are central to the research but not yet described in published literature, software must be made available to editors and reviewers. We strongly encourage code deposition in a community repository (e.g. GitHub). See the Nature Research [guidelines for submitting code & software](#) for further information.

### Data

Policy information about [availability of data](#)

All manuscripts must include a [data availability statement](#). This statement should provide the following information, where applicable:

- Accession codes, unique identifiers, or web links for publicly available datasets
- A list of figures that have associated raw data
- A description of any restrictions on data availability

## Field-specific reporting

Please select the one below that is the best fit for your research. If you are not sure, read the appropriate sections before making your selection.

Life sciences  Behavioural & social sciences  Ecological, evolutionary & environmental sciences

For a reference copy of the document with all sections, see [nature.com/documents/nr-reporting-summary-flat.pdf](https://www.nature.com/documents/nr-reporting-summary-flat.pdf)

## Life sciences study design

All studies must disclose on these points even when the disclosure is negative.

Sample size	For small and robust in vitro experiments: n = 3. For non-efficacy animal studies (e.g. CD45 silencing): n = 5. For the efficacy studies: n = 12 because of the higher level of variation between disease severity. When n was set to 12, the standard deviations were deemed small enough.
Data exclusions	No data was excluded
Replication	All experiments were carried out at least 3 times successfully.
Randomization	Samples and mice were randomized in the experiments
Blinding	Investigators were blinded during randomization and during data acquisition

## Reporting for specific materials, systems and methods

We require information from authors about some types of materials, experimental systems and methods used in many studies. Here, indicate whether each material, system or method listed is relevant to your study. If you are not sure if a list item applies to your research, read the appropriate section before selecting a response.

### Materials & experimental systems

n/a	Involved in the study
<input type="checkbox"/>	<input checked="" type="checkbox"/> Antibodies
<input type="checkbox"/>	<input checked="" type="checkbox"/> Eukaryotic cell lines
<input checked="" type="checkbox"/>	<input type="checkbox"/> Palaeontology and archaeology
<input type="checkbox"/>	<input checked="" type="checkbox"/> Animals and other organisms
<input checked="" type="checkbox"/>	<input type="checkbox"/> Human research participants
<input checked="" type="checkbox"/>	<input type="checkbox"/> Clinical data
<input checked="" type="checkbox"/>	<input type="checkbox"/> Dual use research of concern

### Methods

n/a	Involved in the study
<input checked="" type="checkbox"/>	<input type="checkbox"/> ChIP-seq
<input type="checkbox"/>	<input checked="" type="checkbox"/> Flow cytometry
<input checked="" type="checkbox"/>	<input type="checkbox"/> MRI-based neuroimaging

## Antibodies

### Antibodies used

Rat anti-mouse  $\alpha$ 4 $\beta$ 7 integrin (Clone DATK32, Biolegend)  
 Rat anti-mouse  $\beta$ 7 integrin (Clone FIB504, BioXCell)  
 Mouse anti-rat IgG2a (Clone RG7/1.30, BioXCell)  
 Rat IgG2a isotype control (Clone 2A3, BioXCell)  
 PE-conjugated donkey anti-mouse IgG (Polyclonal, Jackson Immuno Research)  
 AlexaFluor 647-conjugated goat anti-rat IgG (Polyclonal, Biolegend)  
 AlexaFluor 647-conjugated mouse anti-human IgG (Polyclonal, Biolegend)  
 AlexaFluor 647-conjugated rat anti-mouse CD45 (Clone 30-F11, Biolegend)  
 AlexaFluor 488-conjugated rat anti-mouse CD45 (Clone 30-F11, Biolegend)  
 BV650-conjugated rat anti-mouse/human CD11b (Clone M1/70, Biolegend)  
 PE/Cy5-conjugated rat anti-mouse CD19 (Clone 6D5, Biolegend)  
 BV421-conjugated hamster anti-mouse CD3e (Clone 145-2C11, Biolegend)  
 APC/Cy7-conjugated rat anti-mouse CD4 (Clone GK1.5, Biolegend)  
 AlexaFluor 488-conjugated rat anti-mouse CD8a (Clone 53-6.7, Biolegend)  
 PE-conjugated rat anti-mouse CD8a (Clone 53-6.7, Biolegend)  
 PE/Dazzle 594 rat anti-mouse CD25 (Clone PC61, Biolegend)  
 BV510 armenian hamster anti-mouse CD69 (Clone H1.2F3, Biolegend)  
 PE-conjugated rat anti-mouse FOXP3 (Clone MF-14, Biolegend)  
 HRP-conjugated donkey anti-rat IgG (Polyclonal, Jackson Immuno Research)

### Validation

Every antibody was validated for the specific assay it was used for. Antibodies were also checked for cross-reactivity.

## Eukaryotic cell lines

Policy information about [cell lines](#)

Cell line source(s)	American Type Culture Collection
Authentication	None of the cell lines used were authenticated
Mycoplasma contamination	Cell lines were tested negative for mycoplasma contamination every 2 months.
Commonly misidentified lines (See <a href="#">ICLAC</a> register)	No misidentified cell lines were used in the study.

## Animals and other organisms

Policy information about [studies involving animals](#); [ARRIVE guidelines](#) recommended for reporting animal research

Laboratory animals	C57BL/6J wild type and C57BL/6J IL-10KO mice were used in this study.
Wild animals	This study did not use wild animals
Field-collected samples	This study did not involve samples collected from the field
Ethics oversight	The Tel Aviv Institutional Animal Care and Use Committee approved the animal protocols for all in vivo studies in accordance with current regulations and standards of the Israel Ministry of Health.

Note that full information on the approval of the study protocol must also be provided in the manuscript.

## Flow Cytometry

### Plots

Confirm that:

- The axis labels state the marker and fluorochrome used (e.g. CD4-FITC).
- The axis scales are clearly visible. Include numbers along axes only for bottom left plot of group (a 'group' is an analysis of identical markers).
- All plots are contour plots with outliers or pseudocolor plots.
- A numerical value for number of cells or percentage (with statistics) is provided.

### Methodology

Sample preparation	Cells were either taken from cell culture or animal tissues. For tissue appropriate tissue dissociation techniques were used. Single cell suspensions were used for the flow cytometry
Instrument	Beckman Coulter CytoFLEX LX
Software	Kaluza
Cell population abundance	Cells were collected to obtain at least 3000 events in the smallest subpopulation.
Gating strategy	Live cells were gated with DAPI-negative staining. Singlets were gated with SSC-H vs. SSC-A plots. Different cell types were gated with FSC/SSC plots and specific cell populations were gated with the corresponding labeled antibody.

- Tick this box to confirm that a figure exemplifying the gating strategy is provided in the Supplementary Information.